AIP | The Journal of Chemical Physics

Hydrodynamic mechanisms of spinodal decomposition in confined colloid-polymer mixtures: A multiparticle collision dynamics study

Alexander Winkler, Peter Virnau, Kurt Binder, Roland G. Winkler, and Gerhard Gompper

Citation: J. Chem. Phys. **138**, 054901 (2013); doi: 10.1063/1.4789267
View online: http://dx.doi.org/10.1063/1.4789267
View Table of Contents: http://jcp.aip.org/resource/1/JCPSA6/v138/i5
Published by the American Institute of Physics.

Hydrodynamic mechanisms of spinodal decomposition in confined colloid-polymer mixtures: A multiparticle collision dynamics study

Alexander Winkler,[1] Peter Virnau,[1] Kurt Binder,[1] Roland G. Winkler,[2] and Gerhard Gompper[2]
[1]*Insitut für Physik, Johannes Gutenberg-Universität, Staudinger Weg 7, 55099 Mainz, Germany*
[2]*Theoretical Soft Matter and Biophysics, Institute for Advanced Simulation and Institute of Complex Systems, Forschungszentrum Jülich, 52425 Jülich, Germany*

(Received 9 October 2012; accepted 26 December 2012; published online 1 February 2013)

A multiscale model for a colloid-polymer mixture is developed. The colloids are described as point particles interacting with each other and with the polymers with strongly repulsive potentials, while polymers interact with each other with a softer potential. The fluid in the suspension is taken into account by the multiparticle collision dynamics method (MPC). Considering a slit geometry where the suspension is confined between parallel repulsive walls, different possibilities for the hydrodynamic boundary conditions (b.c.) at the walls (slip versus stick) are treated. Quenching experiments are considered, where the system volume is suddenly reduced (keeping the density of the solvent fluid constant, while the colloid and polymer particle numbers are kept constant) and thus an initially homogeneous system is quenched deeply into the miscibility gap, where it is unstable. For various relative concentrations of colloids and polymers, the time evolution of the growing colloid-rich and polymer-rich domains are studied by molecular dynamics simulation, taking hydrodynamic effects mediated by the solvent into account via MPC. It is found that the domain size $\ell_d(t)$ grows with time t as $\ell_d(t) \propto t^{1/3}$ for stick and (at late stages) as $\ell_d(t) \propto t^{2/3}$ for slip b.c., while break-up of percolating structures can cause a transient "arrest" of growth. While these findings apply for films that are 5–10 colloid diameters wide, for ultrathin films (1.5 colloid diameters wide) a regime with $\ell_d(t) \propto t^{1/2}$ is also identified for rather shallow quenches. © *2013 American Institute of Physics*. [http://dx.doi.org/10.1063/1.4789267]

I. INTRODUCTION

When flexible polymers[1] are added to a suspension of non-aggregating spherical colloidal particles, the polymers may create an entropic attraction ("depletion forces"[2,3]) between the colloids. Here, we assume that the colloidal particles are suspended in a fluid that acts as a good solvent for the polymers (or as a Theta solvent, so the polymers assume ideal, random-walk-like conformations[1]). The colloids also have a purely repulsive (almost hard-sphere like[4–6]) interaction at very short distances. Such systems are model systems for the study of collective phenomena in condensed matter, particularly of phase transitions, for several reasons: (i) The interaction range can be tuned by choosing the molecular weight of the polymers, and hence their size (on average, the polymers form soft spherical coils which may overlap each other with little energy penalty), while the strength of the interaction can be controlled by their concentration in the solution. (ii) The colloid particles radii are in the μm range, allowing direct observation of their cooperative structure formation (e.g., via confocal microscopy techniques); for instance, interfaces between coexisting fluid phases[7–9] can be visualized on the single particle level. The dynamics of fluctuations is orders of magnitude slower than that of molecular systems and therefore can often be followed in real time.[7,8,10,11] (iii) Simple theoretical models can be formulated to describe these systems (e.g., Refs. 2 and 12), which are very well suited for simple approximate theories[13,14] and for computer simulations.[15–25] In fact, for a suitable size ratio $q = R_p/R_c$ (R_p being the radius of the soft sphere representing the polymer, R_c the radius of the hard sphere representing the colloidal particle), one predicts that a vapor-liquid type phase separation occurs,[13,14] and this has been confirmed experimentally,[3,26] and both experiments[27] and simulations[19–22] have confirmed the Ising-like critical behavior of such systems.

Since both the interface between the coexisting polymer-rich phase (which would correspond to the "vapor" at a vapor-liquid transition of a simple fluid) and colloid-rich phase, and wetting layers at solid walls are easily observable,[7,9–11] colloid-polymer (cp) mixtures are also well suited to investigate the interplay of finite-size, surface effects, and interfacial phenomena of confined fluids. Many computer simulations exploring the static equilibrium aspects of such phenomena are already available[18,23,24] (see Ref. 24 for a review and further references). We recall that one can argue[24] that for colloid-polymer mixtures it is a good approximation of reality to consider confinement by flat (hard) walls, since the corrugation and roughness of a solid wall on the atomic scale does not play any role for μm-size colloids, unlike the problem of confinement of small molecular fluids in pores.[28] The suggestion has also been made[23,24] that by coating a wall with a polymer brush (where grafting density and chain length of the macromolecules are suitable control parameters) an effective potential is created that selectively repels the colloids, since at a low enough grafting density the polymers in the

suspension may interpenetrate the polymers in the brush, and thus tune the contact angle[29] at which interfaces between unmixed phases meet the wall. Model calculations[25] indicate that in this way wetting properties of walls could be varied all the way from "complete wetting" to "complete drying."[29–31]

Of course, for many aspects of confined multi-component fluids not only the equilibrium phase behavior matters, but also the dynamics of phase separation processes.[32–36] Such kinetic aspects are not only relevant for various applications (micro- and nanofluidic devices,[37–39] oil recovery from porous rocks,[40] separation processes through porous membranes,[41] etc.), but are challenging out-of-equilibrium statistical mechanical processes.[42–46] Hence, simulation studies of phase separation in thin films still is an active area of research.[45,46] Some previous work exists performing simulation studies with molecular dynamics (MD) methods on various models of confined molecular fluids,[47–49] but typically in these studies neither the precise wettability conditions of the confining walls were known, nor could hydrodynamic boundary conditions (b.c.) be varied.

In the present article, we reconsider the dynamics of phase separation processes for colloid-polymer mixtures under confinement, exploring the fact that for suitable models of such systems both bulk properties[12] and wetting at walls[25] have been well characterized. At this point, we note that the original Asakura-Oosawa (AO) model,[2] that was widely studied in early simulations,[14–24] is not suitable for this purpose, since polymers are strictly treated as ideal gas particles having no mutual interactions, an aspect inappropriate for a MD simulation.[50–52] Therefore, an extended version of the AO model was introduced,[12,53] that we henceforth shall call the "continuous Asakura Oosawa" (CAO) model, where polymers interact with a soft, spherically symmetric, simplified model potential (see Sec. II below). As is well-known, invoking known properties for polymers in solution,[6] one could derive such an effective potential,[54] but such an approach would complicate matters unnecessarily, since such a (more accurate) "true" effective potential must depend on solvent quality, polymer concentration in the solution, etc. Being interested in the qualitative aspects of a generic model, we continue to use the model proposed by Zausch *et al.*[12] Also the colloid-colloid (cc) and colloid-polymer interaction is not taken hard-sphere like, as in the original AO model, but replaced by continuous potentials of the Weeks-Chandler-Andersen (WCA) type.[55] As is well-known,[5,6] the idea that the colloid-colloid interaction can be precisely represented by a hard sphere model is a myth rather than reality.

However, even when one aims only at a qualitative description of a generic model, describing the dynamics of this model[12] simply by carrying out MD simulations using the interactions mentioned above, one misses an important physical ingredient: the fluid solvent creates (long range) hydrodynamic interactions among all the colloid particles and polymers. As is well-known for mixtures of small molecules as well as for polymer blends, hydrodynamic interactions have a pronounced effect on the dynamics of domain coarsening in phase-separation processes.[32–36] Experiments on polymer mixtures show that hydrodynamic interactions also matter for surface effects on spinodal decomposition.[56,57] Experiments on the phase-separation kinetics of colloid-polymer mixtures in the bulk[8,58,59] have also given clear evidence for the importance of hydrodynamic interactions, and the experimental exploration of phase separation kinetics for these systems in confined geometry has begun only very recently[60,61] yielding many interesting details which deserve further investigation. We wish to contribute to the understanding of this problem by computer simulation. However, since the size of the solvent molecules is in the nm range, while the size of the colloids is in the μm range, it is impossible to perform a full scale molecular simulation of interacting solvent molecules plus colloids and polymers.

This problem can be circumvented, however, by treating the solvent fluid in a coarse-grained manner by the multiparticle collision dynamics method (MPC).[62–72] In this method, the viscosity of the solvent fluid can be tuned to a desired value, while there are no static correlations of the effective particles which effect the momentum transport: This is appropriate, since on the μm scale of the colloids the structural correlations of the fluid molecules in the solvent are negligible.

The above description has qualitatively summarized the main physical ingredients of the multiscale simulation model that shall be studied in the present work. Section II now describes the model more precisely, and summarizes what is known about its static properties, and discusses an efficient simulation strategy. Section III reports our results, both on domain morphologies and on the observed domain growth laws. A discussion of related work and the theoretical background on the growth laws will be given whenever appropriate. Section IV summarizes our findings.

II. MODEL, STATIC EQUILIBRIUM PROPERTIES, SIMULATION STRATEGY

A. A variant of the Asakura-Oosawa model with continuous potentials

We use an extension of the AO model for colloid-polymer mixtures where all interactions are described by continuous potentials. Hence, MD methods based on numerical integration of Newton's equations of motion can be straightforwardly applied, using the forces computed as derivatives of the pairwise potentials between particles. These potentials for colloid-colloid pairs and for colloid-polymer pairs are taken of the WCA[55] form, i.e., truncated and shifted Lennard-Jones potentials

$$U_{WCA}^{\alpha\beta}(r) = \begin{cases} 4\varepsilon_{\alpha\beta}\left[\left(\frac{\sigma^{\alpha\beta}}{r}\right)^{12} - \left(\frac{\sigma^{\alpha\beta}}{r}\right)^{6} + \frac{1}{4}\right], \\ r < r_c = 2^{1/6}\sigma_{\alpha\beta} \\ 0, \text{ else.} \end{cases} \quad (1)$$

Here, r is the distance between the particles and $\alpha\beta$ describes cc or cp pairs. For the polymer-polymer interaction, we choose instead[12]

$$U^{pp}(r) = \begin{cases} 8\varepsilon_{pp}\left[1 - 10\left(\frac{r}{r_c}\right)^{3} + 15\left(\frac{r}{r_c}\right)^{4} - 6\left(\frac{r}{r_c}\right)^{5}\right], \\ r < r_c = 2^{1/6}\sigma_{pp} \\ 0, \text{ else.} \end{cases} \quad (2)$$

The parameters for the amplitudes $\varepsilon_{\alpha\beta}$ and radii $\sigma_{\alpha\beta}$ are chosen to be the same as in the previous work,[12] namely,

$$\sigma_{cc} = 1.0, \quad \sigma_{cp} = 0.9, \quad \sigma_{pp} = 0.8 \tag{3}$$

and

$$\varepsilon_{cc} = 1.0, \quad \varepsilon_{cp} = 1.0, \quad \varepsilon_{pp} = 0.0625. \tag{4}$$

Hence, the radius of the polymers is about 20% smaller than the colloid radius. We recall that a vapor-liquid type phase separation in the original AO model occurs only if $q = R_p/R_c$ exceeds a value of about $q = 0.25$.[3,13,14,26] The choice $\varepsilon_{cc} = \varepsilon_{cp} = 1.0$ sets the scale for the temperature (we also take Boltzmann's constant $k_B \equiv 1$), and $\sigma_{cc} = 1.0$ is our unit of length. The choice $\varepsilon_{pp} = 1/16$ is clearly arbitrary (more realistic would be a value near $\varepsilon_{pp} = 1/4$)[54] but was chosen for the sake of computational efficiency.[12]

When we consider the confinement between two parallel walls, we choose a rectangular box geometry $L_x \times L_y \times L_z$, with $L_x = L_y = L$ and periodic boundary conditions in x- and y-directions, while two walls are placed at $z_w = \pm L_z/2$. We also choose a WCA potential to describe the effect of the walls, with $\alpha = (c, p)$, for the wall at $z_w = -L_z/2$ it reads explicitly as

$$U^{\alpha}_{\text{wall}}(z) = \begin{cases} 4\varepsilon^{\alpha}_w \left[\left(\frac{\sigma^{\alpha}_w}{z - z_w} \right)^{12} - \left(\frac{\sigma^{\alpha}_w}{z - z_w} \right)^{6} + \frac{1}{4} \right], \\ z_w < z < z_w + 2^{1/6}\sigma^{\alpha}_w, \\ 0 \quad \text{else}, \end{cases} \tag{5}$$

and similarly for the wall at $z_w = +L_w/2$. We choose $\varepsilon^p_w = \varepsilon^c_w = 1$ and $\sigma^c_w = 0.5$, $\sigma^p_w = 0.4$. For this choice, complete wetting of the walls by the colloid-rich phase is expected for a wide range of conditions.[25] In the following, the distance between the walls will be denoted as $D(\equiv L_z)$.

In order to compare the present model to the original AO model, one needs to introduce effective diameters $d^{\alpha}_{\text{eff}}(\alpha = c, p)$ such that the packing fractions η_c and η_p of colloids and polymers correspond to each other, with

$$\eta^{\alpha} = \rho_{\alpha} \left(d^{\alpha}_{\text{eff}} \right)^3 \pi/6, \tag{6}$$

ρ_{α} being the particle number density of species α. It has been shown in Ref. 12 that for the present choice of energy parameters $d^{\alpha}_{\text{eff}} = 1.01557\sigma^{\alpha}$ is an accurate approximation. The polymer density then is controlled by an appropriate choice of the polymer chemical potential μ_p or, equivalently, the so-called "polymer reservoir packing fraction"[2,3,12–14]

$$\eta^r_p = \exp(\mu_p/k_BT) \left(d^p_{\text{eff}} \right)^3 \pi/6. \tag{7}$$

B. Static phase behavior of the model

As has been amply documented in the literature, the static equilibrium phase diagram of such models is most effectively obtained from grand-canonical Monte Carlo simulations,[50,51,73] using cluster moves[19,20] to sample η_c as function of the colloid chemical potential μ at fixed η^r_p over a wide enough range to cross the coexistence curve. Close to phase coexistence with μ near μ_{coex}, the probability distribution $P_{\mu VT}(\eta_c)$ exhibits two maxima that correspond to the coexisting polymer-rich and colloid-rich phases[19,20] ($V = L^2D$ is the volume of the system). Note that for the actual computation of this probability distribution one uses methods such as successive umbrella sampling,[74] and μ_{coex} then is found from the "equal weight rule",[73] i.e., the areas underneath the two peaks describing the coexisting phases are equal. From such a calculation, one can extract the effective free energy function $F/k_BT = -\ln P_{\mu VT}(\eta_c)$ taken for $\mu = \mu_{\text{coex}}$. An example relevant for the present study is given in Fig. 1. Here, the wall separation was chosen so small that in the z-direction no two colloids (nor a colloid-polymer pair) would fit into the system anymore, when they have the same x, y-coordinates, and hence in this case of extreme confinement to an ultrathin slit the configuration is quasi-two-dimensional. Such data are needed to obtain an estimate for the interfacial tension γ, which can be extracted from the free energy excess $\Delta F/k_BT$ in the flat horizontal part in the center of the distribution as[75]

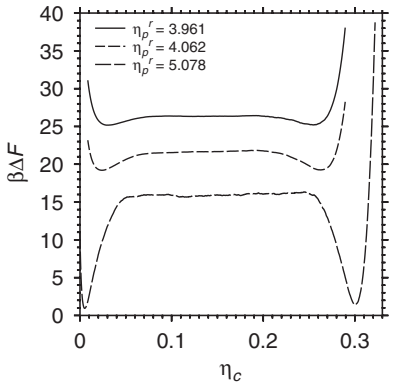

FIG. 1. Free energy function $\Delta F(\eta_c)/k_BT$ plotted vs. η_c for a quasi-two-dimensional system, choosing linear dimensions $L_x = 20$, $L_y = 60$ and $D = 1.5$, for three choices of η^r_p as indicated. In all these cases, μ was adjusted to μ_{coex} (which depends on η^r_p, of course[19,20]). The curves for the two smaller values of η^r_p where moved upward by arbitrary amounts, for better visibility. Note that the choice $L_y = 3L_x$ has advantages for the estimation of the interfacial tension, because then the two interfaces (of area $A = L_xD$) are well separated along the y-axis, and hence do not interact with each other.

$$\gamma = (DL)^{-1} \Delta F/(2k_BT). \tag{8}$$

Note that a factor $1/k_BT$ has been absorbed in γ as well, and a factor 1/2 occurs because there are two interfaces and the normalization of ΔF must be such that $\Delta F = 0$ in the minimum. This interfacial tension is a central driving force for the domain coarsening in the latest stages of phase separation kinetics,[32–36] and hence a calculation as shown in Fig. 1, which yields both the compositions η^v_c, η^{ℓ}_c of the coexisting vapor-like and liquid-like phases of the unmixed colloid-polymer mixture from the positions of the minima, and γ from the maximum in between, is a tedious but necessary prelude to a study of phase separation kinetics. From Fig. 1, we see that even for η^r_p as large as $\eta^r_p \approx 4$ the maximum in the center is very small, so that under such conditions the system is still near its critical point, and Eq. (8) would require the use of very large linear dimensions, which is very difficult. For $\eta^r_p = 5.078$, however, it is

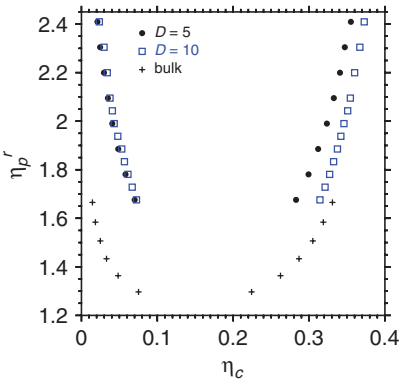

FIG. 2. Phase diagram of the CAO model, comparing the system in the bulk (taken from Ref. 12 shown by crosses) and in the thin film geometry, confined by two planar walls a distance D apart, for $D = 5$ and $D = 10$ (as indicated in the figure). Several linear dimensions of $L_x = L_y = 6.735$, $L_x = L_y = 10$ and $L_x = 8$, $L_y = 20$ were used to exclude noticeable finite-size effects. Symbols indicate the colloid packing fraction in the polymer-rich phase (left branches) and in the colloid-rich phase (right branches).

clear that γ is appreciably different from zero, so one is then far away from criticality, and hence the correlation length of volume fraction fluctuations in equilibrium in any of the pure phases is small, and the data should not be affected by finite-size effects due to the finite values of the lateral linear dimensions.

This example illustrates how we obtain the phase diagrams in the plane of our control variables η_p^r and η_c (Fig. 2). The data of Fig. 2 were all taken from the locations of the corresponding minima of $\Delta F(\eta_c)$, similar as illustrated in Fig. 1. Of course, the two branches of the coexistence curve (the polymer-rich phase, left branch, corresponds to the vapor phase of a simple fluid, the colloid-rich phase, right branch, to the liquid phase) are expected to merge at the critical point. However, a study of the critical region would require a finite-size scaling analysis,[73,76] and this is out of the scope of the present study. In Fig. 2, only such data are included for which lateral finite-size effects are still negligibly small (on the scale of the figure). Of course, this calculation does not only yield η_c for both coexisting phases, but the corresponding values of the polymer volume fraction as well. With this information the phase diagram in the plane of density variables (η_p, η_c) can be constructed (Fig. 3). For a phase diagram where the ordinate is an intensive thermodynamic variable (such as η_p^r, Fig. 2, which is related to μ_p) the tie lines connecting the two coexisting phases must be horizontal and hence the critical point is an extremum (in our case a minimum) of the coexistence curve (Fig. 2). However, the tie lines in Fig. 3 have nontrivial angles with the coordinate axes; no particular symmetry exists for phase diagrams when both variables are densities of extensive variables, of course. With the present simulation methodology particle numbers N_p and N_c of polymers and colloids of the order of a few thousands suffice to yield essentially the phase diagram that would result in the thermodynamic limit; but for the simulations of phase separation kinetics we shall need particle numbers in the range from several hundred thousands to a million.

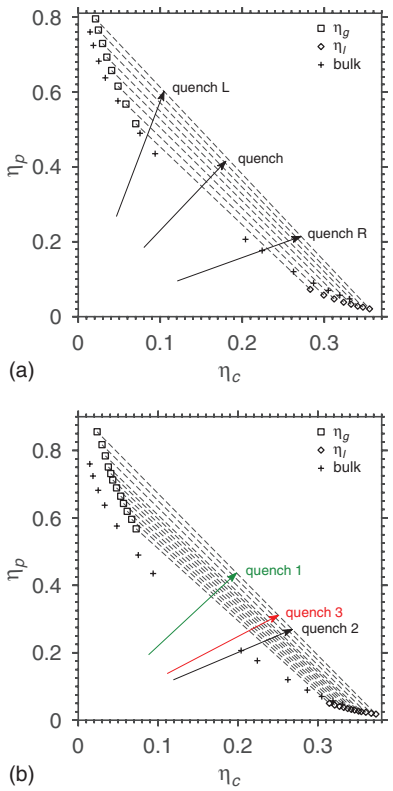

FIG. 3. Phase diagram of the confined CAO model in the plane of variables polymer packing fraction η_p (ordinate) versus colloid packing fraction η_c (abscissa), for $D = 5$ (a) and $D = 10$ (b). Crosses show the corresponding bulk data (taken from Ref. 12). The broken straight lines indicate the tie lines connecting coexisting phases. Arrows indicate the quenches (performed via reduction of the volume at constant particle numbers N_c and N_p of colloids and polymers, respectively, for different ratios N_c/N_p) that will be discussed in Sec. III.

C. Simulation strategy to simulate quenching experiments and incorporating hydrodynamic interactions

We have also indicated by arrows the volume quenches that we consider in Sec. III to prepare initially unstable homogeneous states inside of the coexistence region (which means above the coexistence curve in Fig. 3). Reducing the volume at constant particle number corresponds in Fig. 3 to a straight line passing through the origin, the slope of the straight line being given by the ratio of the particle numbers, N_p/N_c. Experimentally such a quench could be performed by moving the confining walls with a piston against each other until the desired distance is reached, keeping the solvent density constant via an outlet covered by a semipermeable membrane, which is impenetrable for both colloids and polymers only. Of course, also other types of quenches are conceivable (one could keep the volume and the number of colloids N_c as well as the number of solvent molecules constant, and add polymers to the solution, producing an initially unstable homogenous state by stirring the suspension), but are out of consideration here.

In the simulation, the quench is actually performed by a sudden reduction of the linear dimension L at constant D, by rescaling the particle coordinates. Of course, initially some particles will strongly overlap, leading to numerical instabilities of the MD algorithm during the very first time steps due

to the huge forces that drive the particles apart. This problem requires special treatment, restricting the maximum value of the force during the first few time steps artificially. Since the solvent particles act as a very efficient thermostat, this problem automatically disappears after a few time steps. Since an instantaneous volume quench is an idealization (in an experiment, a piston can only be moved with a finite velocity), and we are interested in the dynamics of the system only on time scales that are many orders of magnitude larger than a single time step, this technical difficulty does not matter at all. Note that we keep the solvent density constant, by simply deleting the appropriate number of solvent particles. As a MD algorithm, the well-known velocity Verlet code was used.[50–52] In the MD runs, the masses of polymers and colloids are set to $m_c = m_p = 1$ (thus, the time unit $\tau_{MD} = \sigma_{cc}(m_c/\varepsilon_{cc})^{1/2} = 1$ as well). Of course, in reality $m_c \gg m_p$, but the present choice is made because it is computationally more efficient.

We set the MPC cell size to $a = 0.5\sigma_{cc} = 0.5$. Hence, there are typically many polymers (they are allowed to overlap) in a MPC cell, but only a single colloid. This choice allows us to study hydrodynamic effects already on rather small scales of a few cell sizes.

The stochastic rotation dynamics[62] version of the MPC algorithm is adopted, where the fluid dynamics proceeds in two steps, a streaming and collision step. In the streaming step, the particles move ballistically during the time $\tau_{\rm coll}$, denoted as collision time. In the collision step, MPC particles are sorted into cubic collision cells of side length a. The interaction between the particles within such a cell is achieved by the rotation of their relative velocities with respect to the center-of-mass velocity of a cell around a randomly oriented axis by an angle α. The orientation of the axis is uniformly chosen and independent for every cell and collision step. Thereby, mass and momentum are conserved on the collision cell level. The discretization of space leads to a violation of Galilean invariance, hence, a random shift of the collision lattice is applied.[65] The coupling between the solvent and colloid and polymer particles is established in the collision step, where these particles are included in the MPC collision.[64,67,68,72] Here, their momenta are taken into account in the calculation of a cell's center-of-mass velocity. Since $m_c = m_p$, colloids and polymers are treated as identical. Of course, on the scale of nanoseconds to microseconds colloids and polymers have a very different dynamics; however, being interested in larger times only, the Stokes-Einstein relation implies diffusive dynamics for both particle types, controlled by solvent viscosity and particle radii. The solvent number density controls the compressibility of the MPC solvent. A high value of this parameter, therefore, approximates better an almost incompressible real solvent than a low value, but, of course, the computational effort is increased. Here, a solvent number density of $\rho_s^c = 10$ per cell was chosen which leads to $\rho_s = 80$ per unit volume, and the mass given to a solvent particle was $m_s = 0.025$ (leading to a solvent mass of 2 per unit volume). We use the cell-level canonical Maxwell-Boltzmann-statistics thermostat,[70] which has a high performance and acts very strongly which is an important ingredient in practice to stabilize the system directly after the quench. The coupling between the embedded particles (colloids and polymers) and the solvent is performed by simply including the center of mass of the colloids and polymers in the collision step of the MPC algorithm.

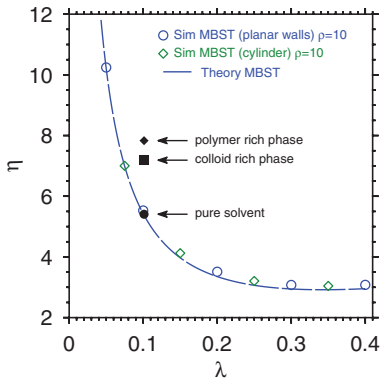

FIG. 4. Shear viscosity η of the pure solvent as a function of the mean free path λ, estimated from a study of Poiseuille flow between walls (open circles) or inside of a cylinder (open diamonds), implementing stick boundary conditions at the walls.[77] The curve shows the corresponding prediction from kinetic theory[63–66] for this case.[77] The full symbols highlight the choice made for the present simulations of phase separation kinetics, including also the estimates of the viscosities in the pure coexisting phases.

Choosing then a collision time step $\tau_{\rm coll} = 4\delta t = 0.008$, $\delta t = 0.002$ being the step of the MD integrator, and the rotation angle $\alpha = 90^\circ$, one obtains a mean free path $\lambda = \tau_{\rm coll}\sqrt{k_BT/(m_s a^2)} \approx 0.1$ and the viscosity of the pure solvent $\eta = \nu\rho_s^c \approx 5.4$ (ν is the kinematic viscosity in units of $\sqrt{k_BTa^2/m}$).[77] Figure 4 shows a plot of the solvent viscosity as function of λ, including also the estimates of the viscosities that result for the two coexisting bulk colloid-rich and polymer-rich phases. These estimates were obtained from studying Poiseuille flow velocity profiles across the slit when a uniform force parallel to the walls is added to the particles, for the case of stick boundary conditions at the walls. Unlike recent studies of phase separation of hexadecane and carbon dioxide,[49,78] where a strong dynamic asymmetry reminiscent of "viscoelastic phase separation"[79] is possible, we find that the viscosities of the two coexisting phases are rather similar, despite the strong asymmetry in their static correlations.[12]

An interesting issue is to convert our dimensionless numbers, such as a shear viscosity $\eta \approx 5\sqrt{m_s k_B T}/a^2$ of our solvent, Fig. 4, to real systems. Of course, in real systems the colloid radius R_c may vary typically from 0.2 μm to 1.0 μm, and hence also the characteristic times τ_R of the diffusive motion of the colloidal particles, defined as $\tau_R = R_c^2/6D = \pi R_c^3\eta/(k_BT)$, vary from about 6η/Pa–760η/Pa at T = 300 K, when the Stokes-Einstein relation is invoked. Assuming a viscosity of the solvent of 10^{-3} Pa s, as is typical for a low-molecular weight organic solvent, this translates into times from 0.006 s to 0.76 s. On the other hand, in our simulation we have chosen units such that the colloid diameter $\sigma_{cc} = 1$, $\varepsilon_{cc} = k_BT = 1$, and the colloid mass $m_c = 1$, and hence the time scale of a molecular dynamics step $\tau_{\rm MD} = \sigma_{cc}(m_c/\varepsilon_{cc})^{1/2} = 1$. When we restore here physical units using $m_c = \rho\sigma_{cc}^3\pi/6$, where $\rho \approx 2 \times 10^3$ kg/m^3 is the mass density (e.g., for silica particles), we find that $\tau_{\rm MD}$ corresponds to 5×10^{-4} s and 10^{-6} s for $\sigma_{cc} \approx 10^{-6}$ m and 2×10^{-7} m,

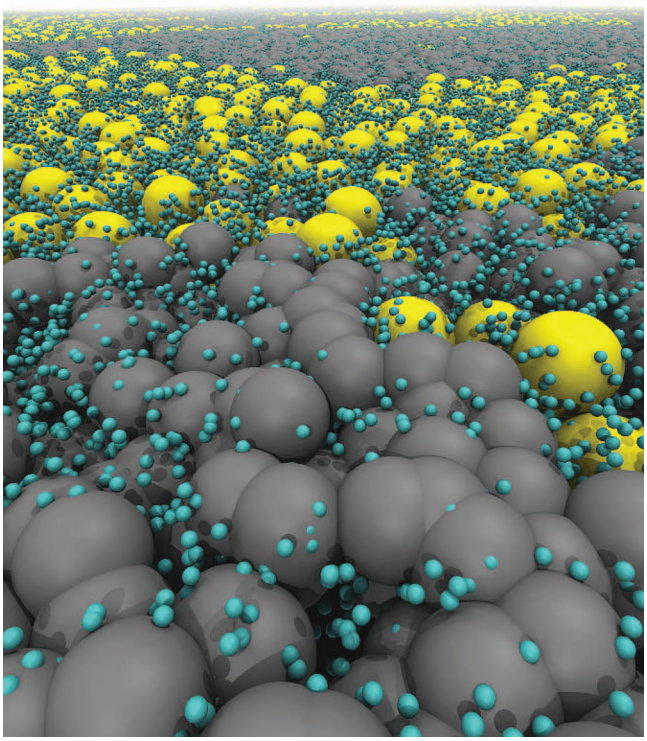

FIG. 5. Snapshot of the colloids and polymers during the demixing process visualizing the three different length scales: the point-like solvent particles (shown in blue), the colloids and polymers (shown in yellow and black respectively) as well as the length scale of the colloid-rich and polymer-rich domains. The snapshot corresponds to an ultrathin film of thickness $D = 1.5$ at $\eta_p^r = 5.078$. For a clearer view on the large domains, a layer containing many solvent particles was removed from the top. Solvent particles inside the colloids and polymers are also not visible.

respectively. Hence, we obtain characteristic times of the order of $\tau_R = 10^3 \tau_{\rm MD}$ for the above range of colloid radii. On the other hand, the MPC viscosity $\eta \approx 5\sqrt{m_s k_B T}/a^2$ leads to a characteristic time $\tau_R = \pi R_c^3 \eta/(k_B T) \approx \tau_{\rm MD}$. Hence, we obtain a speed-up of the motion of a colloidal particle by three orders of magnitude in comparison with the real system. Of course, this choice of a significantly smaller viscosity η (in comparison with the real system) is dictated by the need of an efficient simulation algorithm.

Since we expect a complex behavior describing the linear dimension $\ell_d(t)$ of the growing domains, with $\ell_d(t) \gg \sigma_{cc}$ in the later stages of the phase separation resulting from the quenches indicated in Fig. 3, we need to simulate systems with very large linear dimensions L parallel to the walls, to avoid finite-size effects. We have chosen $L = 256$ for $D = 5$ and $D = 10$ (and occasionally even $L = 512$ for $D = 1.5$) throughout. In order to provide a visual impression of such a phase separating system on the particle level, Fig. 5 shows a typical snapshot. To carry out such a simulation of a very large system over several orders of magnitude in time (more than 10^4 MD time units), a fast code implementation for the massively parallel supercomputer HERMIT[80] was developed, running the code on up to 4096 processors of this CRAY XE6 machine in parallel (more details about the performance and parallelization model are given in the Appendix).

We end this section with a comment on the hydrodynamic boundary conditions that the solvent particles experience at the walls. As is well-known,[63–70] via appropriate rules for the momentum change when solvent particles are reflected at the walls one can straightforwardly implement perfect slip or perfect stick boundary conditions. In the slip case, hydrodynamic interactions between the growing domains are not screened, while in the stick case backflow of particles near the walls is drastically reduced. Hence, we expect that on large length-scales hydrodynamic interactions are progressively screened out the smaller the wall distance D. Note that the slip boundary condition is simply obtained by specular reflection of the solvent particles at the walls, while the stick boundary condition results from "bounce back" reflections. Also partial slip could be realized[81] but has not been implemented here. It is also possible to switch off the hydrodynamic interactions completely. Instead of the explicit solvent particles of the MPC method, in each MPC cell a momentum drawn from a Maxwell-Boltzmann distribution with zero mean and variance $\sigma^2 = m_s M k_B T$ (M is the number of particles per cell)[82] is used. In this way, thermal fluctuations via this thermostat are still included.

III. SIMULATION RESULTS ON PHASE SEPARATION KINETICS

A. Extracting characteristic lengths $\ell_d(t)$ describing domain growth

In quenching simulations of binary fluids confined into thin films, it is known from previous studies of related models[47–49] that during the early stages of the time evolution after the quench, a complicated interplay between phase separation in the z-direction across the film (due to the possible formation of precursors of wetting or drying layers) and the coarsening of domains that extend over large distances in the lateral (x, y)-directions occurs. In the present study, the stages of this lateral coarsening is our main focus. For this reason, the regions near the walls (in the case of thin films with $D = 5$ and $D = 10$) are excluded from the analysis, in order to eliminate the effect of these wetting or drying layers. For instance, for the wall distance $D = 10$, seven slices with a width of 0.5 in the range $z \in [-1.75, +1.75]$ were used. In each slice, a quasi-two-dimensional pair correlation function is calculated taking only x- and y-components of the particle positions into account. The seven resulting pair correlation functions are then averaged. For $D = 5$, only three such slices of width 0.5 were used. Figure 6 shows typical data for this radial pair correlation function for the middle quench shown in Fig. 3(a), which is performed for $\eta_p/\eta_c \approx 2.3$ and thus almost passes the critical point. Note that for this choice the quench leads to a state where both colloids and polymers are in the middle of the miscibility gap, which would be at $\eta_c = (\eta_c^v + \eta_c^\ell)/2$ and $\eta_p = (\eta_p^v + \eta_p^\ell)/2$ since the two end points of the tie line in Fig. 3 are (η_c^v, η_p^v) and $(\eta_c^\ell, \eta_p^\ell)$. This is the analog of the "critical quench" in models such as the kinetic Ising model[32–36] or the symmetric binary Lennard-Jones mixture,[48] where quenches through the critical point (in the bulk) automatically ensure equal amounts of both

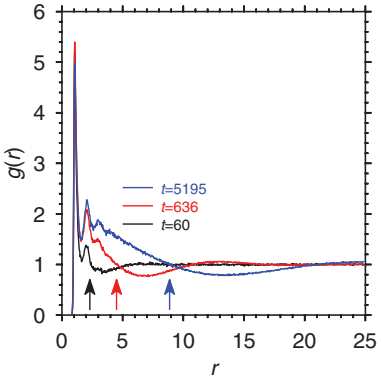

FIG. 6. Radial pair distribution function $g(r, t)$ of the colloids in lateral direction ($r = \sqrt{x^2 + y^2}$) for $D = 5$ at a quench to the state with $(\eta_c^v, \eta_p^v) = (0.0234, 0.775)$ and $(\eta_c^\ell, \eta_p^\ell) = (0.350, 0.0239)$. Three times after the quench are shown, as indicated. Arrows indicate the choice of $r_{c2}(t)$, see text. These data refer to the choice of stick boundary conditions.

coexisting phases throughout the phase separation process. We see in Fig. 6 the typical oscillations of $g(r)$ at small distances, resulting from the structure that is formed by rather dense packing of (almost) hard particles. However, while in equilibrium these oscillations decay rather fast and $g(r) = 1$ when r exceeds a few colloid diameters, we see here a large-scale structure developing. $g(r, t)$ develops a shallow minimum at $r = r_{\min}(t)$ where $g(r_{\min}(t), t) < 1$, and this minimum position moves outward to larger and larger r as $t \to \infty$. Due to the features of this shallow minimum and statistical noise in the data, it would require a very large computational effort to locate the minimum precisely; however, it is much easier to obtain the location of the second intersection of $g(r, t)$ with the horizontal line at unity, and hence we take this intersection as a measure of the domain size,

$$g(r = r_{c2}(t), t) = 1, \quad \ell_d(t) = 2.5 r_{c2}(t). \tag{9}$$

Here, the factor 2.5 is introduced because then $\ell_d(t)$ approximately coincides with $\ell_m(t) = 2\pi/q_m(t)$ extracted from the peak of the structure factor. It also would be possible to consider a two-dimensional Fourier transformation $S(\vec{q})$ of the colloid-colloid correlations and locate the position $q_m(t)$ where the (circularly averaged) structure factor $S(q)$ has its maximum.[32–36] However, since $S(\vec{q})$ is not self-averaging,[83] such data typically are much more noisy than $\ell_d(t)$ as defined in Eq. (9),[49,77,78] and hence shall not be reported here.

B. Growth behavior for films of several colloidal diameters in width

Being interested in the influence of hydrodynamic interactions on phase separation, we start by presenting a series of typical snapshots of the time evolution of the domain configuration (Fig. 7), for cases where slip or stick boundary conditions were used, and for the case where hydrodynamic interactions were completely switched off (by the use of a cell-wise momentum drawn from a Maxwell-Boltzmann distribution, see Sec. II). As expected, right after the quench ($t = 12$) hydrodynamic interactions have no effect, the system is still essentially homogenous, apart from small-scale

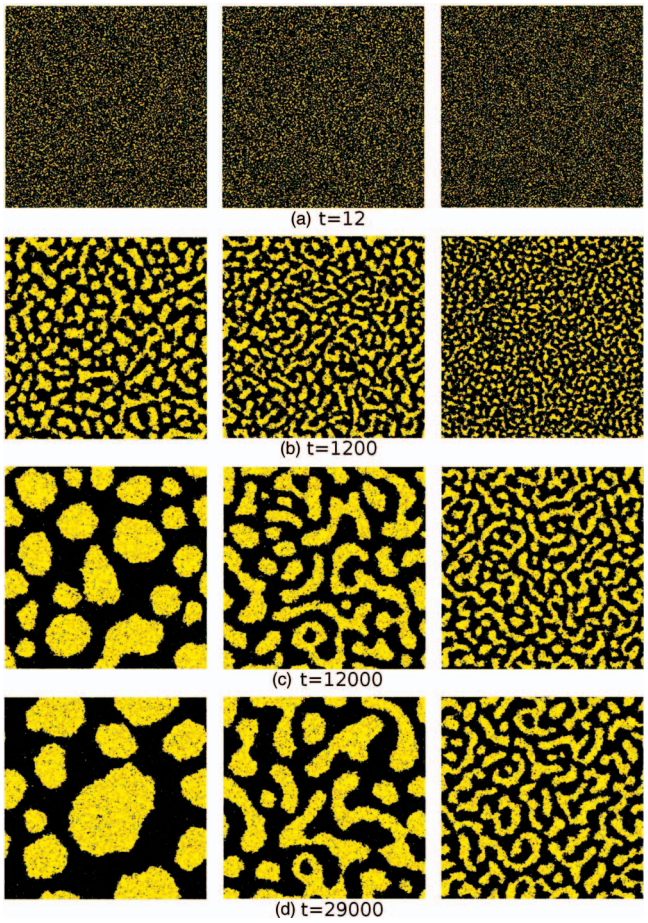

FIG. 7. Snapshots of the demixing process, showing times $t = 12$ (a), 1200 (b), 12 000 (c) and 29 000 (d) MD time units after the quench. Only xy-coordinates of the polymer positions of a $256 \times 256 \times 5$ system are shown as black dots (the colloids are shown in yellow). The data are for the "critical quench" as characterized in Fig. 6, and refer to slip boundary conditions (left), stick boundary conditions (middle) and switched-off hydrodynamics (right).

packing fraction inhomogeneities. At the time $t = 1200$, in all three cases the typical irregular percolating seaweed-like structure has formed, familiar from many studies of kinetic Ising models, time-dependent Ginzburg-Landau models or symmetric binary mixtures.[32–36,49,78] But already at these intermediate times it is obvious that the model without hydrodynamics evolves much slower. Of course, this conclusion is fully expected from the general knowledge about hydrodynamic effects in fluids and fluid mixtures,[84] and for spinodal decomposition in the bulk a regime where $\ell_d(t)$ grows linearly with time[85] in favorable cases is reached rapidly.[86] This linear growth law has also been demonstrated experimentally for colloid-polymer mixtures.[58,59] Different growth laws were predicted by Dhont,[87] but apply at best at intermediate stages. Also when a phase-separating thin film is embedded in a bulk (three-dimensional) fluid, hydrodynamic effects are well documented.[88] However, for confined films[44,47–49] and in the strictly two-dimensional case[78,89–95] the domain growth laws in the presence of hydrodynamic interactions have remained controversial. Without hydrodynamic interactions, one expects on the basis of the Lifshitz-Slyozov evaporation-condensation mechanism, where large

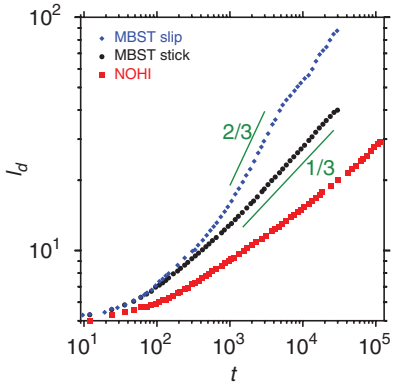

FIG. 8. Domain size $\ell_d(t)$ vs. time t, for the "critical quench" of Figs. 6 and 7 in the film of thickness $D = 5$, and the three choices of dynamics: slip boundary conditions, stick boundary conditions, and switched-off hydrodynamics. Straight lines illustrate growth exponents of 1/3 and 2/3, respectively, on this log-log plot.

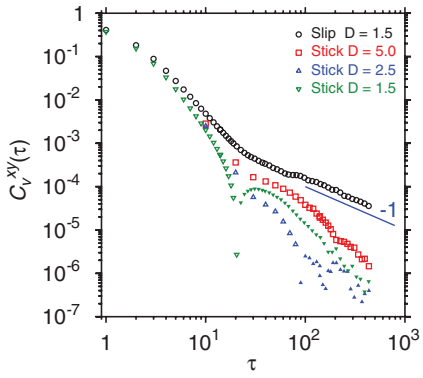

FIG. 9. Two-dimensional velocity autocorrelation functions plotted versus collision time steps $\tau = 0.008$ on a log-log plot, for various wall distances D and boundary conditions, as indicated. Full symbols mark negative values, i.e., an anticorrelation of the velocity over time.

droplets grow on the expense of smaller ones, a growth law $\ell_d(t) \propto t^{1/3}$, irrespective of dimensionality.[32–36,89] In a fluid, Stokes diffusion of droplets and their coagulation[90,91] implies $\ell_d(t) \propto t^{1/3}$ in $d = 3$ as well, while $\ell_d(t) \propto t^{1/2}$ in $d = 2$. The latter law has also been proposed in Ref. 92. However, it has been pointed out[93,94] that both in $d = 2$ and $d = 3$ the ultimate growth law should be ruled by a growth exponent of 2/3,

$$\ell_d(t) \propto t^{2/3}, \quad \text{if } \ell_d(t) > \ell_{\text{in}} = \eta^2/(\rho\gamma). \tag{10}$$

Here, the "inertial length" ℓ_{in} needs to be exceeded (here, ρ is the total fluid density). This growth law should apply when the inertial term in the Navier-Stokes equation describing the fluid hydrodynamics dominates over the viscous part.[34,93,94] So far, there exists no experimental evidence for Eq. (10) yet, to the best of our knowledge. But the possibility has also been raised that different measures of the structural inhomogeneity in $d = 2$ evolve with different growth exponents[95] invalidating the idea that phase separation kinetics in $d = 2$ is ruled by a simple scaling description with a universal growth exponent. In any case, Fig. 7 shows that for the system studied here full hydrodynamic interactions produce a much faster growth, and in the late stages also a change from the interconnected morphology of the domains to almost circular domains occurs.

When we analyze now the growth laws resulting for the system shown in Fig. 7 for $\ell_d(t)$ vs. t (Fig. 8), we see that both the case without hydrodynamics and with stick boundary conditions shows a very slow, transient growth for $\ell_d(t) \leq 10$, while for $\ell_d(t) > 10$ the effective exponent is close to 1/3. This finding could be interpreted as the Lifshitz-Slyozov mechanism to apply in both cases, but the diffusion of the particles from the smaller domains to the larger ones is somewhat speed up, in a fluid in which hydrodynamic interactions are screened at large distances due to the stick boundary conditions at the walls. Most interesting, of course, is the behavior for the slip boundary condition, where the growth exponent 2/3 indeed can be observed for about a decade in time ($10^3 \leq t \leq 10^4$), before a crossover to a slower growth ($\approx$1/2) occurs. This crossover goes along with the crossover of the morphology from interconnected almost percolating structures to well-separated domains.

These interpretations are supported by a direct study of velocity autocorrelation functions of the fluid particles for stick or slip boundary conditions in very thin films (Fig. 9). Indeed, for the slip case we observe the long time tail, $C_v^{xy}(\tau) \propto \tau^{-1}$, characteristic for a fluid in $d = 2$. With stick boundary conditions, the velocity correlations at late time are progressively screened as D becomes smaller. Note that the data of Fig. 9 were taken in a pure fluid system in equilibrium, no colloids or polymers being present. The differences between the autocorrelations become pronounced on time scales of order 100τ or larger. For the solvent viscosity under consideration with a mean free path of $\lambda \approx 0.1$, this corresponds to a length scale of the order of 10 which is the length where the domain growth laws start to exhibit significant differences between the stick and slip case (Fig. 8).

It remains to comment why in the case where hydrodynamic interactions are completely switched off the 1/3 growth exponent sets in only after a very long transient regime in Fig. 8. In order to test this behavior, we have repeated a simulation of this case where the density of fluid particles was taken an order of magnitude smaller, which reduces the fluid velocity and thereby accelerates the demixing process: then[77] indeed the $\ell(t) \propto t^{1/3}$ growth law is observed earlier. Thus, the interpretation for the slow crossover seen in Fig. 8 simply is that for the case without hydrodynamics the friction due to the high-density solvent particles slows down the diffusive motion of the colloids and polymers.

Both for film thickness $D = 5$ and $D = 10$, we observe for times t up to about $t = 10^3$ MD time units slow transients, which show up with a rather pronounced curvature of the function $\ell_d(t)$ vs. t in the log-log plot. It is then a natural question to ask to what extent this behavior might correlate with the formation of colloid-rich precursors of wetting layers at the walls during these stages, as observed in simulations of phase separation of molecular systems under similar conditions.[47–49]

To answer this question, we show in Fig. 10 snapshots of the early stages of quench 1 (see Fig. 3(b)), where side views of a slice of thickness $\delta = 8$ of the film are shown for six times as indicated. Figure 10(b) shows additionally the top view (xy-plane) of the domain structure at MD time

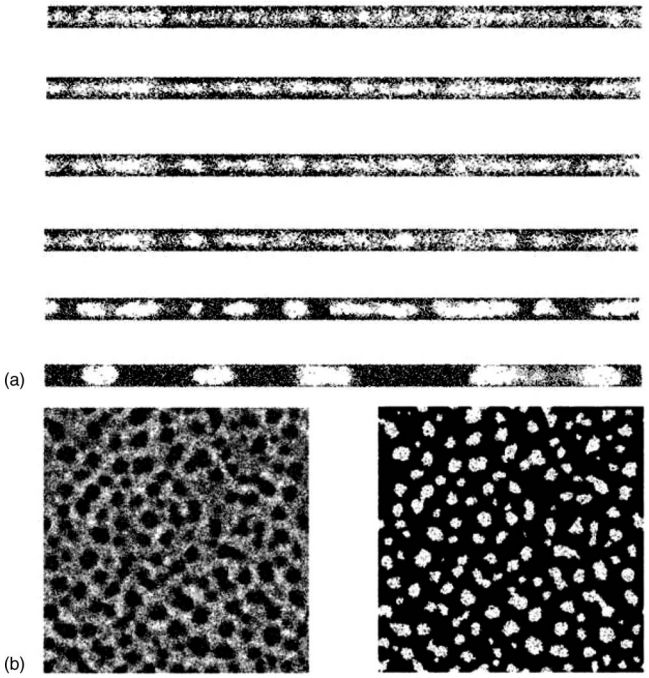

FIG. 10. Early stages of the demixing process for quench 1 in the system with wall distance $D = 10$ and slip boundary condition. (a) Side view on a center slice of width 8 for several times: (from top to bottom) 228, 540, 936, 1224, 1512, 6306. Here, colloids are represented as black dots, while the polymers are not shown. (b) Top view of the system at time $t = 1512$ where at the left only the colloids are shown as black dots and at the right only the polymers are shown as black dots.

$t = 1512$ for both the colloids (left) and polymers (right). Indeed, for times $t > 1000$ one can distinguish well-separated polymer-rich and colloid-rich domains, and in the side views there is a clear evidence that the interfaces separating these domains are not just running straight from one wall to the other, but exhibit a curved meniscus, such that colloids get enriched at the walls. This is expected, since for a bulk system ($D \to \infty$) for the chosen complete wetting conditions, the walls would be coated by colloid-rich wetting layers throughout (which cannot happen in the considered very thin films, of course). However, this surface enrichment of colloids at the walls is responsible for the fact that there is a clear majority of the polymer-rich phase in the central slice near $z = 0$ for the "critical" quench considered here. The colloid-rich phase in the central slice looks like an assembly of many disconnected droplets, while the polymer-rich phase clearly percolates. This partial phase separation between polymers and colloids in the z-direction builds up gradually at times $t \lesssim 1000$ after the quench, and is one reason for the slow transient for the lateral domain growth. Similar observations have been made for other quenches.

Having identified physical reasons for the slow transient seen in the variation of $\ell_d(t)$ in Fig. 9, we discuss a phenomenological analysis[86] which allows one to better identify the asymptotic growth law. This method is based on the concept of an offset length l_s, which is subtracted from $\ell_d(t)$ to define the new length scale $\ell' \equiv \ell_d(t) - l_s$. This offset length is not an arbitrary fit parameter, but defined such that the effective time-dependent exponent α_t

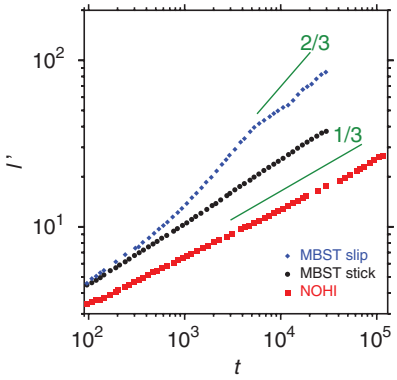

FIG. 11. Reduced average domains size $\ell'(t) = \ell_d(t) - \ell_s$ for the system with wall distance $D = 5$ for all three b.c. (compare with Fig. 9).

$$\alpha_t \equiv \frac{\partial \ln \ell'(t)}{\partial \ln t} \tag{11}$$

is essentially independent of t for large t. It turns out that for our model this condition is roughly fulfilled (we note that estimation of α_t by numerical differentiation of data as shown in Fig. 16 involves appreciable statistical errors) if $l_s = 2.5$ is chosen. This value is still a microscopic length of the order of the range over which the correlation function in Fig. 6 still exhibits the typical packing oscillations. Note that the same value applies irrespective of the presence of hydrodynamic interactions and the choice of boundary conditions. Therefore, we consider this choice of l_s as reasonable. Figure 11 shows that now the simple diffusive growth (no hydrodynamic interactions) is compatible with the relation $\ell'(t) \propto t^{1/3}$ over three orders of magnitude in time. For the case where hydrodynamic interactions are present, we have a slightly larger effective exponent in the case of stick b.c., while for the case of slip b.c. the two crossovers are still present, as in the original data (Fig. 9). We recall that the $\ell'(t) \propto t^{2/3}$ law can only be found when $\ell_d(t)$ exceeds the inertial length, so that a single exponent for $\ell_d(t)$ or $\ell'(t)$ over the whole range of times cannot be expected and that the slow-down from $t \approx 5000$ on is due to the change in pattern morphology. We also note that the behavior for films with such mesoscopic thickness as $D = 5$ or $D = 10$ may be complicated, since the system is in a sense in-between dimensionality $d = 2$ and $d = 3$ with respect to the correlations.

Figure 12 illustrates the effect of variation of relative concentration of the polymer-rich and colloid-rich phases. As shown by the snapshots, both for 25:75 and for 75:25 relative concentrations one has a droplet morphology, with either a colloid-rich droplets phase on a polymer-rich background, or vice versa. Although the viscosities of the pure polymer-rich and colloid-rich phases are not completely identical, the curves $\ell_d(t)$ vs. t almost coincide. Despite the presence of hydrodynamic interactions in the case of slip boundary conditions, the growth law is the same as that of a system with symmetric composition (50:50) but with stick rather than slip boundary conditions.

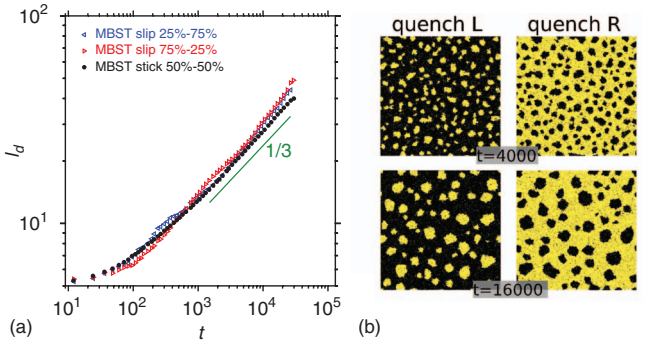

FIG. 12. (a) Domain size $\ell_d(t)$ vs. time t, for two off-critical quenches with relative concentration 75:25 (L) and 25:75 (R) of the polymer-rich and colloid-rich phases, studied with slip boundary conditions for wall distance $D = 10$. For comparison, the system with 50:50 concentrations (but studied with stick rather than slip boundary conditions) is included, to show that all these systems evolve with a growth exponent of about 1/3 (indicated by the straight line). (b) Corresponding snapshots for the two quenches (L,R), as described in part (a) and indicated also in Fig. 3(a), for time $t = 4000$ and $t = 16\,000$.

Next, we consider the effects of film thickness on the growth behavior. For $D = 10$ several quenches varying the relative concentrations of both phases were made (as indicated already in Fig. 3(b)). Since for this larger value of D more pronounced wetting layers of the colloids form at both walls, the nominally critical quench (at symmetric 50:50 composition) actually leads to a droplet morphology of the colloid-rich phase already during the early stages (Fig. 13(a), denoted as quench 1). For a significantly higher colloid fraction (quench 2 in Figs. 3(b) and 13(a)), the colloid-rich phase stays percolating throughout the time evolution, but now it is the polymer-rich phase which shows a transition from an interconnected morphology to droplets (Fig. 13(a), middle part). It turns out that in the time evolution of $\ell_d(t)$ this leads to a transient "arrest" of the growth, exemplified by a sharp kink in the $\ell_d(t)$ vs. t log-log-plot. As a caveat, however, we mention that these data (Fig. 13(c)) refer to a single realization of the system only; one might expect that taking averages over many independent time realizations, this break up of the interconnected structure will not occur at precisely the same time in the different samples, and so the kink will be smoothed out. For a somewhat smaller colloid fraction (quench 3 in Figs. 3(b) and 13(a)), the interconnected character of the structure persists, and then the time evolution of the growth at late times is well compatible with the $t^{2/3}$ law (Fig. 13(c)). It turns out that for the quantification of the morphology of the patterns it is useful to consider the Euler characteristic.[96,97] For this purpose, a mapping on the two-dimensional Ising model is performed, introducing (virtual) subsystems of size 4×4, in which the average order parameter is computed, and put to one if it exceeds $(\eta^v(t) + \eta^\ell(t))/2$ and equal to zero if it is smaller (for either kind of particles, colloids or polymers).[104] In this way, every configuration of a slice parallel to the walls can be reduced to an arrangement of droplets and holes. Every droplet contributes with $\chi = 1$, every hole with $\chi = -1$, and a bicontinuous structure leads to $\chi = 0$. For each configuration, the average Euler characteristic can be computed in this way. The Euler characteristic for both

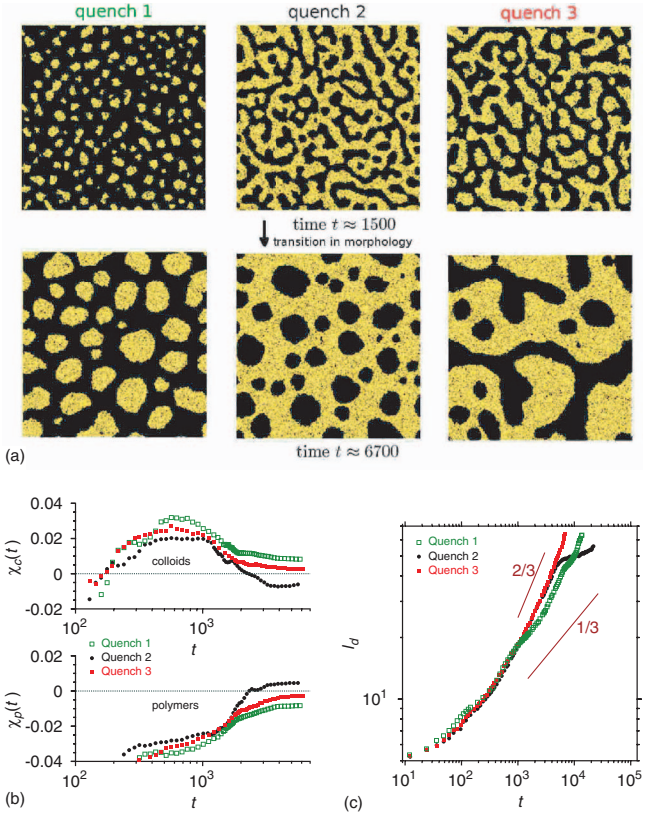

FIG. 13. (a) Snapshots at time $t = 1500$ (upper row) and at time $t = 6700$ (lower row) for the three quenches 1, 2, 3 shown in Fig. 3(b). Only the polymers are shown, as black dots. (b) Average Euler characteristic of colloids $\chi_c(t)$, upper part, and of polymers, $\chi_p(t)$, lower part, plotted vs. time, for the three quenches 1, 2, 3 shown in Figs. 3(b) and 13(a). All runs have been made with slip boundary conditions. (c) Domain size $\ell_d(t)$ on a log-log plot versus time, for the three quenches of Figs. 3(b) and 13(a). Straight lines illustrate the growth law exponents 2/3 and 1/3, as indicated. System sizes were $256 \times 256 \times 10$ throughout.

colloids $\chi_c(t)$ and polymers $\chi_p(t)$ is shown in Fig. 13(b), and these data confirm that it is quench 3 that has both $\chi_c(t)$ and $\chi_p(t)$ near zero for large t. At time $t \geq 700$ the hole-droplet symmetry between the colloid-rich phase and the polymer-rich phase becomes visible in the Euler characteristic, indicating that the subsystems used for the mapping onto the Ising model are distinctively smaller than the average domain size. From this time on, the order parameter peaks in the probability distribution function of each subsystem are clearly distinguishable and hence, allow for a precise decision whether this subsystem is mapped to the value 1 or 0, respectively.

C. Ultrathin quasi-two-dimensional films

Most illuminating is the study of an extremely thin film of thickness $D = 1.5$, which yields insight into the strictly two-dimensional behavior of the model. We choose here a particularly large lateral dimension, $512 \times 512 \times 1.5$, to safely exclude finite-size effects. Motivated by Fig. 1, we perform both a quench at $\eta_p^r = 4.062$ (which corresponds to the critical region, the interfacial tension is very small, $\gamma \approx 0.1$) and at $\eta_p^r = 5.078$ (where $\gamma \approx 0.5$). Using slip boundaries, in both cases the evolution towards rather large domains can be

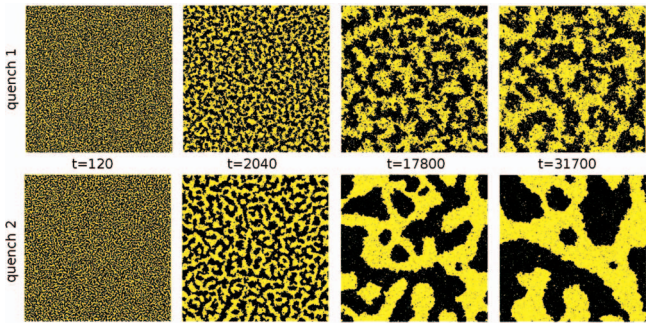

FIG. 14. Comparison of the time evolution of the domain patterns for $\eta_p^r = 4.062$ (upper row) and $\eta_p^r = 5.078$ (lower row), for the 512 × 512 × 1.5 system, and slip boundary conditions.

followed (focusing again on a "critical quench" only). However, for $\eta_p^r = 4.062$ the domain boundaries are extremely rugged, corresponding to diffuse interfaces (Fig. 14), while for $\eta_p^r = 5.078$ the domains are much more compact and the interfaces are sharp. Figure 15 shows that in the case where hydrodynamic interactions are present (using slip boundary conditions at the walls), one finds a relation $\ell_d(t) \propto t^{1/2}$ for $\eta_p^r = 4$ but $\ell_d(t) \propto t^{2/3}$ for $n_p^r = 5$. This difference can be attributed to the fact that for $\eta_p^r = 4.062$ the inertial length $\ell_{\text{in}} = \eta^2/(\rho\gamma)$ is very large, due to the smallness of $\gamma(\approx 0.1)$. Hence, all data fall in the regime where $\ell_d(t) \ll \ell_{\text{in}}$ and

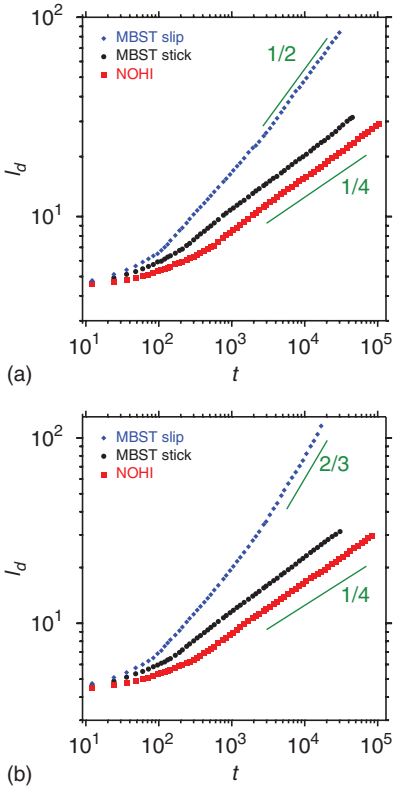

FIG. 15. Average domain size $\ell_d(t)$ vs. t for the 512 × 512 × 1.5 system and the choice $\eta_p^r = 4.062$ (a) and $\eta_p^r = 5.078$ (b). In each case, slip boundary conditions lead to the fast growth with a growth exponent 1/2 (a) or 2/3 (b), while for both the stick boundary condition and in the case of switched-off hydrodynamics, the effective growth exponent exceeds 1/4 only slightly, as indicated by the straight lines.

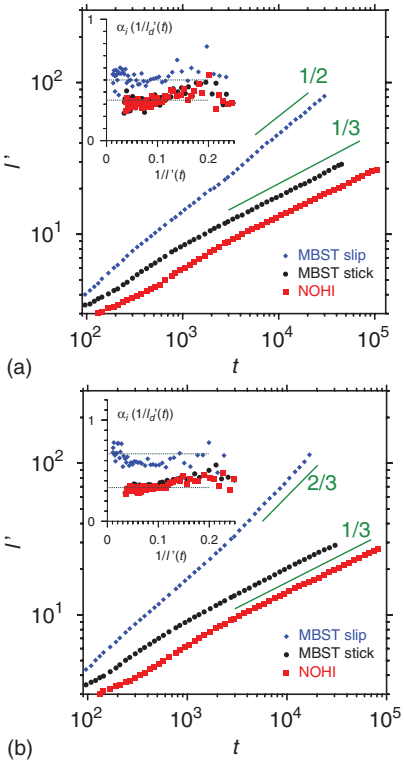

FIG. 16. Reduced average domain size $\ell' = l_d - \ell_s$ with $\ell_s = 2.5$ for a system with $D = 1.5$ and $\eta_p^r = 4.062$ (a) and $\eta_p^r = 5.078$ (b). The insets show the effective exponent α_i (see Eq. (11)) as a function of inverse reduced domain size $\ell'(t)$. Horizontal dotted lines are located at 1/2 and 1/3 (a) and 2/3 and 1/3 (b) serving as a guide to the eye.

therefore $\ell_d(t) \propto t^{1/2}$ is expected indeed (see Eq. (10)). For $\eta_p^r = 5.078$, where γ is about 5 times larger, it seems that the crossover from $\ell_d(t) \propto t^{1/2}$ to $\ell_d(t) \propto t^{2/3}$ falls within the "window" of observable domain sizes.

Omitting all prefactors of order unity in the estimate $\ell_{\text{in}} = \eta^2/(\rho\gamma)$, the values $\eta \approx 5.5$, $\rho \approx 2$ and $\gamma \approx 0.5$ in our units translate into $\ell_{\text{in}} \approx 60$, i.e., a value still below the lateral size of our simulation box. Restoring physical units, $\gamma \approx 0.5$ corresponds to an ultra-low surface tension of about 2×10^{-9} J/m^2, while ℓ_{in} is only 6×10^{-5} m. As noted above, we use an unphysically small solvent viscosity, which is, however, necessary to speed up the simulation. This disparity of scales for the viscosity makes the experimental observation of the regime $\ell(t) \gg \ell_{\text{in}}$ difficult.

At first sight, it is somewhat disturbing that in the case of stick boundary conditions (for this small value of D this means that hydrodynamic effects are suppressed to a large extent) and when hydrodynamics is switched off the apparent growth exponent is almost as low as 1/4. However, we recall that in the kinetic Ising models a very slow approach to the Lifshitz-Slyozov growth exponent 1/3 was also observed, as $\ell_d(t) \to \infty$.[98] Originally, it was suggested[98] that one encounters strong corrections to scaling, so the effective growth exponent is $n_{\text{eff}} = 1/3 - \text{const}/\ell_d(t)$. Alternatively, it has been suggested[86] to analyze the transformed variable $\ell'(t) = \ell_d(t) - \ell_d(t_0)$ instead of $\ell_d(t)$ vs. t. In Subsection III B, we have seen that such an analysis is indeed useful for the present model as well, and for films of thickness $D = 5$ an offset

length of $l_s = 2.5$ was obtained. Applying this analysis for the present quasi-two-dimensional case of $D = 1.5$, we also find that $l_s = 2.5$ is again the proper choice.

Figure 16 is the counterpart of Fig. 15, when we plot $\ell'(t)$ rather than $\ell_d(t)$: Indeed, we now get rid off the problem that the diffusive growth (without hydrodynamic interactions) is characterized by an effective exponent close to 1/4. Instead, a clear evidence in favor of the Lifshitz-Slyozov exponent 1/3 is obtained. Slip b.c., on the other hand, yield a rather clear evidence for $\ell'(t) \propto t^{1/2}$ in the case of shallow quenches (Fig. 16(a)) and $\ell'(t) \propto t^{2/3}$ for deep quenches (Fig. 16(b)). Thus, the behavior observed in our model is in accord with the theoretical expectations.

IV. CONCLUSIONS

We have considered the kinetics of phase separation in colloid-polymer mixtures confined between parallel impenetrable walls. Given the fact that colloidal particles are in the μm size range, we have considered distances D between the walls of such slit pores in the range from 1.5 to 10 colloid diameters. The equilibrium phase behavior of these systems has been investigated separately by appropriate Monte Carlo computer simulations (Figs. 1–3), since the knowledge of colloid and polymer packing fractions in the coexisting phase is an important ingredient both for the set up of the simulation of a volume quenching experiment and for the interpretation of the subsequent domain growth. In such a quench, the packing fractions of both species are enhanced by the same factor, thus, bringing the system from the one-phase region into the two-phase region (Fig. 3), keeping the density of the molecular solvent in this suspension constant.

Since the domain linear dimensions of interest are in the size range from 10 to 100 colloid diameters (cf. Figs. 7, 8, 12, and 13), systems with large lateral linear dimensions (up to $L = 512$ choosing the colloid diameter as unit of length) had to be used. On the other hand, in order to account for the effect of the solvent on the dynamics, using a physically reasonable choice of solvent viscosity (Fig. 4), we needed to apply the MPC method with a large number (namely, 80) fluid particles per unit length (10 particles per MPC cell). Our largest system thus contained more than 52×10^6 solvent particles (typical numbers of colloids and polymers then were $N_c = 236\,859$, $N_p = 1\,019\,022$). Hence, it is clear that such a multiscale simulation requires a huge computational effort, which was only possible due to the use of a massively parallel and highly efficient supercomputer.

A main interest of this study was to test the importance of hydrodynamic mechanisms on the kinetics of phase separation under confinement. As extreme limiting cases, we have assumed perfect slip boundary conditions or perfect stick boundary conditions at the confining walls, as far as the solvent fluid is concerned. Note that we assume such hydrodynamic boundary conditions in a completely phenomenological way, and discuss neither the problem how to realize them experimentally for the considered system, nor to derive them theoretically.[99–102] For comparison, we also consider the case where all hydrodynamic effects are switched off (artificially), so that the collisions of colloids and polymers with the fluid particles act only as a Maxwell-Boltzmann thermostat. Then these fluid particles have no velocity autocorrelations at all, while these correlations are fully developed in the perfect slip case (Fig. 9), and for stick boundary conditions are progressively screened out at large times.

The characteristic domain size $\ell_d(t)$ in the xy-directions parallel to the walls is extracted from the radial pair distribution function in planar slices in the center of the slit pore (Fig. 4), and correlated with the connectivity (or lack thereof) of the domain pattern seen in the corresponding "snapshots" of the system configurations. The typical growth laws that reflect hydrodynamic effects in $d = 2$ dimensions, namely, $\ell_d(t) \propto t^{1/2}$ or $\ell_d(t) \propto t^{2/3}$ (Fig. 15) are only found when perfect slip boundary conditions are used. Stick boundary conditions as well as simulations where hydrodynamic effects are switched off are both compatible with a Lifshitz-Slyozov type law $\ell(t) \propto t^{1/3}$, Fig. 8. The latter relation is also found for "off-critical" quenches, when either polymers or colloids assume a clear droplet morphology during the growth (Figs. 12 and 13), even if slip boundary conditions are used.

In the first few decades of time after the quench, the growth of the lateral length scale $\ell_d(t)$ is accompanied by the build-up of concentration inhomogeneities in the z-direction perpendicular to the walls, i.e., a precursor effect to the growth of colloid-rich wetting layers. This process causes a slow transient in the growth laws for lateral growth.

We like to stress that there are still some aspects of our findings which are not fully understood. For example, one would have expected that in the off-critical case with perfect slip the two-dimensional droplet diffusion plus coagulation mechanism (leading to $t^{1/2}$) would appear, but this is not the case. In addition, for very thin films ($D = 1.5$) when stick boundary conditions are used one expects the Lifshitz-Slyozov mechanism to be present, but the small effective exponents in Fig. 15 indicate an unexpectedly slow approach towards the asymptotic regime. This problem is removed when the transformation from $\ell_d(t)$ to $\ell'(t) = \ell_d(t) - \ell_s$ with $\ell_s = 2.5$ is made, but the interpretation of ℓ_s in this case is not fully clear.

In conclusion, we hope that our study stimulates some experimental work on this model system. While experiments on phase-separation kinetics of colloid-polymer mixtures in $d = 3$ dimensions are hampered by gravity effects,[8,58,59] and therefore "clean" conditions are only established if one carries out these experiments in the space laboratory,[59] the gravity effect should be negligible for thin films where the z-axis is oriented along the direction of the gravitational force. Consequently, our simulations indicated that colloid-polymer mixtures confined between planar smooth walls, which realize slip boundary conditions (or at least partial slip) should be a suitable model system in which the existence of the $t^{2/3}$ domain growth law could be tested experimentally. To our knowledge, no experimental evidence in favor of this growth law has yet been found in any other system, and therefore a study of this problem is rather desirable. Complementary theoretical studies applying analytical methods would also be welcome.

ACKNOWLEDGMENTS

A. W. thanks the Deutsche Forschungsgemeinschaft (DFG) for support under Grant No. N°TR6/A5 and the FZ Jülich, Institute for Advanced Simulation and Institute of Complex Systems for the hospitality during several research stays. We are grateful to the John von Neumann Institute (NIC Jülich) and the Hochleistungsrechenzentrum Stuttgart (HLRS) for generous grants of computer time on the JUROPA, JUGENE, and HERMIT supercomputers. We are also grateful to A. Statt (Mainz), C.C. Huang (Jülich), and G. Sutmann (Jülich) for their help with some aspects of this project.

APPENDIX: REMARKS ON PARALLELIZATION AND PERFORMANCE OF THE MPC ALGORITHM

At this point a few remarks on the parallelization technique and on the performance of the MPC algorithm are given. The system is divided into subsystems where each of these subdomains has to communicate at the borders with the neighboring subsystems. This is achieved by adding "halo" layers to the borders which contain all the necessary information from the neighboring domain to perform the velocity Verlet integration step. The communication is performed via MPI. The collision step of the solvent is implemented following Ref. 103. When a MPC cell is shared by multiple processes, the necessary information (positions and velocities) is sent in a serial manner in x-direction, y-direction, and z-direction. After the collision is performed, the resulting velocities (positions are not needed anymore) are sent back in the opposite order. This technique allows for a proper treatment of corners and is simple to implement. In comparison to standard molecular dynamics simulations, where no explicit solvent particles are present, the combined MD and MPC algorithm exhibits nearly the same performance when simulations are performed in the late stages of phase separation of an asymmetric binary mixture (in our case only about 10% slower). This comes simply from the fact that the performance of the velocity Verlet step of molecular dynamics algorithms depends strongly on how dense the system is in each subdomain. The most dense subdomain (here, the polymer-rich phase has a significantly higher density in comparison to the colloid-rich phase) sets the performance of the simulation. In addition to this load imbalance, the performance of the MD force calculation depends on the size of the underlying MD cell system, which simply gets too large when the simulation box is divided into very small subsystems. Both of these performance issues of the MD part of the simulation are not present in case of the solvent. The solvent particles are homogeneously distributed in the simulation box so that each process has approximately the same computational effort for the collision and streaming steps of the solvent particles. Furthermore, there exist no force calculation which depends on the MD cell system size for the solvent, so that small subsystems (minimum is one MPC cell) are in principle possible. The homogeneity of solvent-related calculations hides the performance drop down of the MD part of the simulation at late stages and hence, explains why in our special case up to 52×10^6 additional solvent particles come at a very small performance loss.

[1] P. C. de Gennes, *Scaling Concepts in Polymer Physics* (Cornell University Press, Ithaca, NY, 1979).
[2] F. Oosawa and S. Asakura, J. Chem. Phys. **22**, 1255 (1954).
[3] W. C. K. Poon, J. Phys.: Condens. Matter **14**, R859 (2002).
[4] P. N. Pusey, in *Liquids, Freezing, and Glass Transition*, edited by J. P. Hansen, D. Levesque, and J. Zinn-Justin (North-Holland, Amsterdam, 1991), p. 763.
[5] W. C. K. Poon, E. R. Weeks, and C. P. Royall, Soft Matter **8**, 21 (2012).
[6] C. P. Royall, W. C. K. Poon, and E. R. Weeks, Soft Matter **9**, 17 (2013).
[7] D. G. A. L. Aarts, M. Schmidt, and H. N. W. Lekkerkerker, Science **304**, 847 (2004).
[8] D. G. A. L. Aarts, R. P. A. Dullens, and H. N. W. Lekkerkerker, New J. Phys. **7**, 40 (2005).
[9] Y. Hennequin, D. G. A. L. Aarts, J. O. Indekeu, H. N. W. Lekkerkerker, and D. Bonn, Phys. Rev. Lett. **100**, 178305 (2008).
[10] D. G. A. L. Aarts, H. N. W. Lekkerkerker, H. Guo, G. Wegdam, and D. Bonn, Phys. Rev. Lett. **95**, 164503 (2005).
[11] H. N. W. Lekkerkerker, V. W. A. de Villeneuve, J. W. J. de Folter, M. Schmidt, Y. Hennequin, D. Bonn, J. O. Indekeu, and D. G. A. L. Aarts, Eur. Phys. J. B **64**, 341 (2008).
[12] J. Zausch, P. Virnau, K. Binder, J. Horbach, and R. L. C. Vink, J. Chem. Phys. **130**, 064906 (2009).
[13] H. N. W. Lekkerkerker, W. C. A. Poon, P. N. Pusey, A. Stroobants, and P. Warrem, Europhys. Lett. **20**, 559 (1992).
[14] J. M. Brader, R. Evans, and M. Schmidt, Mol. Phys. **101**, 3349 (2003).
[15] M. Dijkstra, J. M. Brader, and R. Evans, J. Phys.: Condens. Matter **11**, 10079 (1999).
[16] M. Dijkstra and R. van Roij, Phys. Rev. Lett. **89**, 208303 (2002).
[17] P. G. Bolhuis, A. A. Louis, and J.-P. Hansen, Phys. Rev. Lett. **89**, 128302 (2002).
[18] M. Schmidt, A. Fortini, and M. Dijkstra, J. Phys.: Condens. Matter **15**, S3411 (2003).
[19] R. L. C. Vink and J. Horbach, J. Chem. Phys. **121**, 3253 (2004).
[20] R. L. C. Vink and J. Horbach, J. Phys.: Condens. Matter **16**, 3807 (2004).
[21] R. L. C. Vink, J. Horbach, and K. Binder, J. Chem. Phys. **122**, 134905 (2005).
[22] R. L. C. Vink, J. Horbach, and K. Binder, Phys. Rev. E **71**, 011401 (2005).
[23] A. De Virgiliis, R. L. C. Vink, J. Horbach, and K. Binder, Europhys. Lett. **77**, 60002 (2007).
[24] K. Binder, J. Horbach, R. L. C. Vink, and A. De Virgiliis, Soft Matter **4**, 1555 (2008).
[25] A. Statt, A. Winkler, P. Virnau, and K. Binder, J. Phys.: Condens. Matter **24**, 464122 (2012).
[26] S. M. Ilett, A. Orrock, W. C. K. Poon, and P. N. Pusey, Phys. Rev. E **51**, 1344 (1995).
[27] B.-H. Chen, B. Payandeh, and M. Robert, Phys. Rev. E **62**, 2369 (2000).
[28] L. Gelb, K. Gubbins, R. Radhakrishnan, and M. Sliwinska-Bartkowiak, Rep. Prog. Phys. **62**, 1573 (1999).
[29] J. S. Rowlinson and B. Widom, *Molecular Theory of Capillarity* (Clarendon, Oxford, 1982).
[30] S. Dietrich, in *Phase Transitions and Critical Phenomena*, edited by C. Domb and J. L. Lebowitz (Academic, London, 1988), Vol. 12, p. 1.
[31] D. Bonn, J. Eggers, J. Indekeu, J. Meunier, and E. Rolley, Rev. Mod. Phys. **81**, 739 (2009).
[32] A. J. Bray, Adv. Phys. **43**, 357 (1994).
[33] K. Binder and P. Fratzl, in *Phase Transformation in Materials*, edited by G. Kostorz (Wiley-VCH, Weinheim, 2001), p. 409.
[34] A. Onuki, *Phase Transition Dynamics* (Cambridge University Press, Cambridge, 2002).
[35] R. C. Desai and R. Kapral, *Dynamics of Self-organized and Self-assembled Structures* (Cambridge University Press, Cambridge, 2009).
[36] *Kinetics of Phase Transitions*, edited by S. Puri and V. Wadhavan (CRC, Boca Raton, 2009).
[37] R. D. Piner, J. Zhu, F. Xu, S. Hong, and C. A. Mirkin, Science **283**, 661 (1999).
[38] Y. Gogotsi, J. A. Libera, A. Güvenc-Yazicioglu, and C. M. Megandis, Appl. Phys. Lett. **79**, 1021 (2001).
[39] T. M. Squires and S. R. Quake, Rev. Mod. Phys. **77**, 977 (2005).
[40] *Handbook of Porous Solids*, edited by F. Schlüth, K. S. W. Sing, and J. Weitkamp (Wiley-VCH, Weinheim, 2002).

[41] S. M. Auerbach, K. A. Carrado, and P. K. Dutta, *Handbook of Zeolite Science and Technology* (Marcel Dekker, New York, 2003).
[42] K. Binder, J. Non-Equilib. Thermodyn. **23**, 1 (1998).
[43] S. Puri, J. Phys.: Condens. Matter **17**, R101 (2005).
[44] K. Binder, S. Puri, S. K. Das, and J. Horbach, J. Stat. Phys. **138**, 51 (2010).
[45] P. K. Jaiswal, S. Puri, and S. K. Das, Europhys. Lett. **97**, 16005 (2012).
[46] P. K. Jaiswal, K. Binder, and S. Puri, Phys. Rev. E **85**, 041602 (2012).
[47] S. K. Das, S. Puri, J. Horbach, and K. Binder, Phys. Rev. Lett. **96**, 016107 (2006).
[48] S. K. Das, S. Puri, J. Horbach, and K. Binder, Phys. Rev. E **73**, 031604 (2006).
[49] K. Bucior, L. Yelash, and K. Binder, Phys. Rev. E **77**, 051602 (2008).
[50] M. P. Allen and D. J. Tildesley, *Computer Simulation of Liquids* (Clarendon, Oxford, 1987).
[51] *Monte Carlo and Molecular Dynamics of Condensed Matter*, edited by K. Binder and G. Ciccotti (Italian Physical Society, Bologna, 1996).
[52] D. C. Rapaport, *The Art of Molecular Dynamics Simulation*, 2nd ed. (Cambridge University Press, Cambridge, 2004).
[53] J. Zausch, J. Horbach, P. Virnau, and K. Binder, J. Phys.: Condens. Matter **22**, 104120 (2010).
[54] P. Bolhuis and A. A. Louis, Macromolecules **35**, 1860 (2002).
[55] J. D. Weeks, D. Chandler, and H. C. Andersen, J. Chem. Phys. **54**, 5237 (1971).
[56] G. Krausch, Mater Sci. Eng. R. **14**, 1 (1995).
[57] M. Geoghegan and G. Krausch, Prog. Polym. Sci. **28**, 261 (2003).
[58] N. A. M. Verhaegh, J. S. van Duijneveldt, J. K. G. Dhont, and H. N. W. Lekkerkerker, Physica A **230**, 409 (1996).
[59] A. E. Bailey *et al.*, Phys. Rev. Lett. **99**, 205701 (2007).
[60] E. A. Jamie, R. P. Dullens, and D. G. Aarts, J. Phys.: Condens. Matter **24**, 284120 (2012).
[61] E. A. Jamie, R. P. Dullens, and D. G. Aarts, J. Phys. Chem. B **115**, 13168 (2011).
[62] T. Ihle and D. Kroll, Phys. Rev. E **63**, 020201 (2001).
[63] A. Malevanets and R. Kapral, J. Chem. Phys. **110**, 8605 (1999).
[64] A. Malevanets and R. Kapral, J. Chem. Phys. **112**, 7260 (2000).
[65] T. Ihle and D. M. Kroll, Phys. Rev. E **67**, 066705 (2003).
[66] T. Ihle, E. Tüzel, and D. M. Kroll, Phys. Rev. E **72**, 046707 (2005).
[67] M. Ripoll, M. Mussawisade, R. G. Winkler, and G. Gompper, Phys. Rev. E **72**, 016701 (2005).
[68] G. Gompper, T. Ihle, D. M. Kroll, and R. G. Winkler, Adv. Polym. Sci. **221**, 1 (2009).
[69] H. Noguchi and G. Gompper, Phys. Rev. E **78**, 016706 (2008).
[70] C. C. Huang, A. Chatterji, G. Sutmann, G. Gompper, and R. G. Winkler, J. Comput. Phys. **229**, 168 (2010).
[71] A. Lamura, G. Gompper, T. Ihle, and D. Kroll, EPL **56**, 319 (2001).
[72] R. Kapral, Adv. Chem. Phys. **140**, 89 (2008).
[73] D. P. Landau and K. Binder, *A Guide to Monte Carlo Simulation in Statistical Physics* (Cambridge University Press, Cambridge, 2009).
[74] P. Virnau and M. Müller, J. Chem. Phys. **120**, 10925 (2004).
[75] K. Binder, Phys. Rev. A **25**, 1699 (1982).
[76] *Finite Size Scaling and Numerical Simulation of Statistical Systems*, edited by V. P. Privman (World Scientific, Singapore, 1990).
[77] A. Winkler, Ph.D. dissertation, Johannes Gutenberg Universität Mainz, 2012 (unpublished).
[78] D. Reith, K. Bucior, L. Yelash, P. Virnau, and K. Binder, J. Phys.: Condens. Matter **24**, 115102 (2012).
[79] H. Tanaka, J. Phys.: Condens. Matter **12**, R207 (2000).
[80] See http://www.hlrs.de/systems/platforms/cray-xe6-hermit/ for more details about the HERMIT supercomputer.
[81] J. K. Whitmer and E. Luijten, J. Phys.: Condens. Matter **22**, 104106 (2010).
[82] M. Ripoll, R. G. Winkler, and G. Gompper, Eur. Phys. J. E **23**, 349 (2007).
[83] A. Milchev, K. Binder, and D. W. Heermann, Z. Phys. B **63**, 521 (1986).
[84] J. M. Ortiz de Zarate and J. V. Sengers, *Hydrodynamic Fluctuations in Fluids and Fluid Mixtures* (Elsevier, Amsterdam, 2006).
[85] E. D. Siggia, Phys. Rev. A **20**, 595 (1979).
[86] S. Ahmad, S. K. Das, and S. Puri, Phys. Rev. E **82**, 040107 (2010).
[87] J. K. G. Dhont, J. Chem. Phys. **105**, 5112 (1996).
[88] S. Ramachandran, S. Komura, and G. Gompper, EPL **89**, 56001 (2010).
[89] I. M. Lifshitz and V. V. Slyozov, J. Phys. Chem. Solids **19**, 35 (1961).
[90] K. Binder and D. Stauffer, Phys. Rev. Lett. **33**, 1006 (1974).
[91] K. Binder, Phys. Rev. B **15**, 4425 (1977).
[92] M. San Miguel, M. Grant, and J. D. Gunton, Phys. Rev. A **31**, 1001 (1985).
[93] H. Furukawa, Phys. Rev. A **31**, 1103 (1985).
[94] H. Furukawa, Phys. Rev. A **36**, 2288 (1987).
[95] A. J. Wagner and J. M. Yeomans, Phys. Rev. Lett. **80**, 1429 (1998).
[96] K. Mecke, Phys. Rev. E **53**, 4794 (1996).
[97] K. Mecke, Eur. Phys. J. B **8**, 99 (1999).
[98] D. A. Huse, Phys. Rev. B **34**, 7845 (1986).
[99] D. A. Edward, H. Brenner, and D. T. Wasan, *Interfacial Transport Processes and Rheology* (Butterworth-Heinemann, Boston, 1991).
[100] H. Brenner and V. Ganesan, Phys. Rev. E **61**, 6879 (2000).
[101] M. M. Denn, Annu. Rev. Fluid Mech. **33**, 265 (2001).
[102] H. C. Öttinger, J. Non-Newtonian Fluid Mech. **152**, 66 (2008).
[103] G. Sutmann, R. G. Winkler, and G. Gompper, "Simulating hydrodynamics of complex fluids: Multi-particle collision dynamics coupled to molecular dynamics on massively parallel computers" (unpublished).
[104] The time-dependent "coexistence densities" $\eta^v(t)$ and $\eta^\ell(t)$ are simply the peak positions of the density distribution in the 4×4 subsystems. It turned out that this did not influence the values of the Euler characteristic which means that the local time-dependent "coexistence densities" converge in a symmetric manner to the (final) equilibrium coexistence densities η^v and η^ℓ.